Scramjets

M. Smart
Centre for Hypersonics,
The University of Queensland,
Brisbane, Australia

ABSTRACT

The supersonic combustion ramjet, or scramjet, is the engine cycle most suitable for sustained hypersonic flight in the atmosphere. This article describes some of the challenges facing scramjet designers, and the methods currently used for the calculation of scramjet performance. It then reviews the HyShot 2 and Hyper-X flight programs as examples of how sub-scale flights are now being used as important steps towards the development of operational systems. Finally, it describes some recent advances in three-dimensional scramjets with application to hypersonic cruise and multi-stage access-to-space vehicles.

NOMENCLATURE

A	area (m^2)
C_f	skin friction coefficient
c_p	specific heat (J/kgK)
C_T	thrust coefficient = $C_T = \dfrac{T}{1/2\rho V_0^2 A_0}$
d	injector hole diameter (m)
D	hydraulic diameter (m)
f_{st}	stoichiometric ratio
F	stream thrust (N)
F_{add}	additive drag (N)
F_{un}	uninstalled thrust (N)
g	gravitational acceleration (ms^{-2})
G	combustor gap height (m)
h	enthalpy (0K basis) (J/kg)
h_{pr}	heat of combustion (J/kg of fuel)
H_t	total enthalpy (0K basis) (J/kg)
Isp	specific impulse (s)
M	Mach number
m_c	mass capture ratio
m	mass flow rate (kg/s)
p	pressure (Pa)
q	dynamic pressure (Pa)
Q	heat (J)
R	gas constant (J/kgK)
T	temperature (K); thrust (N)
T_t	total temperature (K)
V	velocity (ms^{-2})
x	axial distance (m) or direction
x_L	length for complete mixing (m)
α	angle-of-attack (degrees)

Paper No. 3219. Manuscript received 13 July 2007.
This is the latest in a series of invited survey papers focusing on a specific aspect of the aerospace industry.

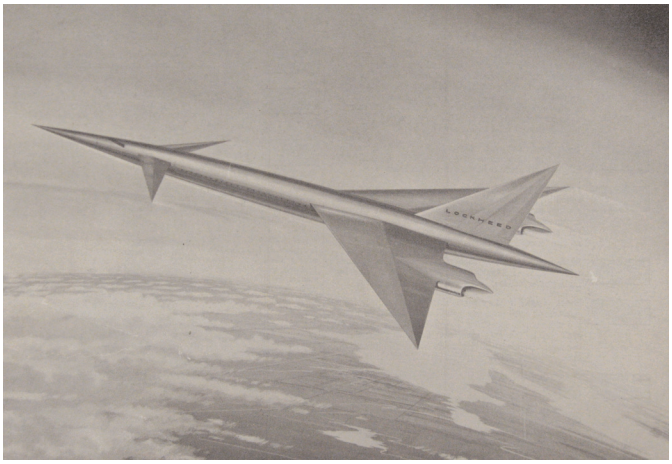

Figure 1. 1960s hypersonic aircraft.

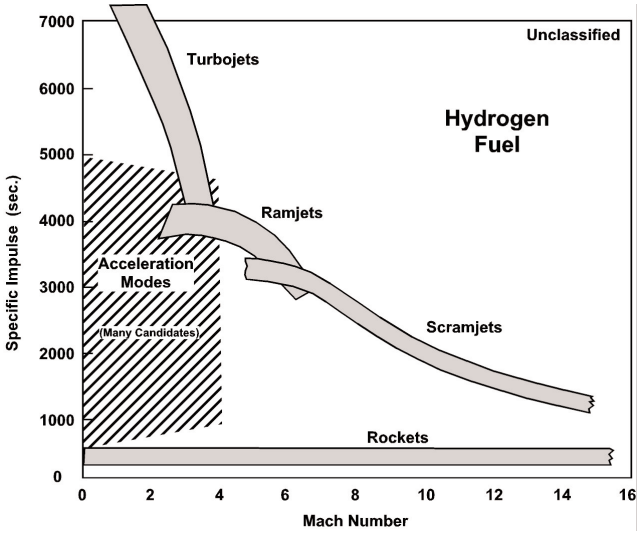

Figure 2. Specific impulse levels for different propulsion systems (NASA).

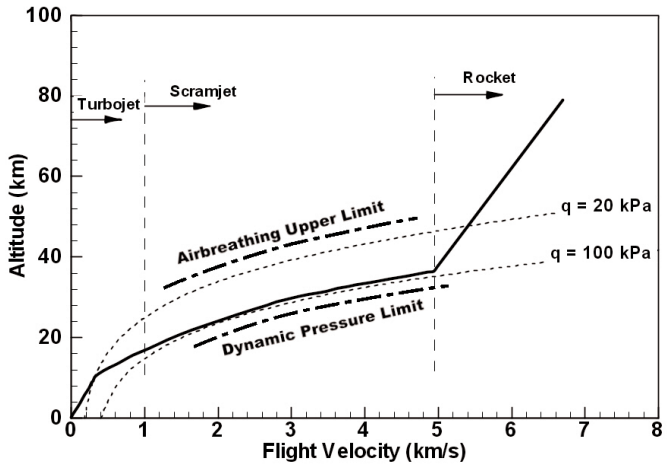

Figure 3. Hypersonic airbreathing flight corridor.

ϕ	equivalence ratio
ϑ	constant in mixing curve
γ	ratio of specific heats
η	efficiency
η_{KE}	kinetic energy efficiency
ρ	density (kg/m^3)
τ	shear stress (Pa)

Subscript

av	average
c	combustor entrance; cowl
e	end of combustor
f	fuel
i	initial
in	inflow
m	mixing
n,*N*	nozzle
out	outflow
w	wall

1.0 INTRODUCTION

The desire for hypersonic flight within the atmosphere has motivated multiple generations of aerodynamicists, scientists and engineers. In the late 1950s and early 1960s it became clear that while rocket propulsion had the potential for access-to-space and the ability to reach many parts of the globe on ballistic trajectories, only an airbreathing propulsion system could facilitate practical hypersonic flight. Antonio Ferri aptly described the important differences between rockets and airbreathing engines[11] as:

1. The potential specific impulse of airbreathing propulsion is much larger than any chemical rocket, due to the fact it carries only fuel and not oxidiser.
2. Structural weight of an airbreathing engine is larger for the same thrust than a rocket, because it must process air (oxygen and nitrogen) and have an intake, whereas the rocket has an oxidiser tank and pressurisation system.
3. The thrust of an airbreathing engine is a function of flight Mach number and altitude. Large thrust per unit frontal area can only be obtained in the dense atmosphere, while rockets can operate at high thrust per unit frontal area in a vacuum.
4. The necessity for flight in the atmosphere introduces severe structural problems for the airbreathing engine associated with aerodynamic heating and vehicle drag. However, the vehicle has a greater potential for manoeuvring than a rocket traveling in a vacuum, through the use of aerodynamic lift.

It was recognised at the time that a hypersonic airbreathing propulsion system could fulfill many roles that a rocket could not, including hypersonic cruise and recoverable space launchers. Figure 1 shows a futuristic hypersonic airbreathing vehicle concept from that time period.

The airbreathing engine cycle best suited to hypersonic flight is the supersonic combustion ramjet, or scramjet. This type of engine can be properly viewed as an extension of the very successful ramjet engine cycle, which uses shock wave compression in the inlet in lieu of the compressor in a gas-turbine engine. In a ramjet, air entering the combustor is first decelerated to subsonic speeds, where fuel is injected and burnt, and finally expanded through a second throat to a thrust nozzle. As flight speeds increase above Mach 5, reducing the air to subsonic conditions produces two problems; (1) significantly increased shock losses in the inlet, particularly at the terminal normal shock, and (2) significantly increased flow temperatures in the combustor. The second of these problems not only creates material/structural issues in the combustor, but also leads to chemical dissociation in the nozzle expansion and a consequent energy loss from the engine cycle.

https://doi.org/10.1017/S0001924000004796 Published online by Cambridge University Press

The idea of adding heat to a supersonic stream was first investigated in the late 1940s, but only attracted serious attention in the late 1950s with the investigation by Weber and McKay (1958)[39] at the NASA Lewis Research Center. This work compared the estimated performance of the ramjet and scramjet engine cycles at increasing Mach number using hydrogen fuel, and calculated that the scramjet cycle was superior above Mach 7. Results of a further study of the efficiency of airbreathing engines[1] are shown in Fig. 2. Once again the switch over between ramjet and scramjet cycles was calculated to occur at Mach 6-7, however it was also pointed out in the same reference that the high combustor static pressure of a ramjet operating above Mach 5 may be a more important reason for choosing a scramjet cycle than fuel efficiency. As speeds increase the specific impulse of scramjets reduces, and is shown in Fig. 2 to reach the performance level of a rocket somewhere above Mach 16.

The flight corridor for scramjet propelled vehicles, either for cruise or ascent to low-earth-orbit, is constrained at upper altitude by the need to operate the airbreathing engine, and at lower altitude by structural limits of the vehicle. Figure 3 gives an indication of these limits, and includes a suggested ascent trajectory for an airbreathing access-to-space vehicle, with turbojet operation up to Mach 3-4, scramjet operation up to Mach 15-17 and then rocket based propulsion for the final boost to low earth orbital velocity, which is approximately 7·9km/s.

Early researchers quickly grasped the difficulties of designing scramjet engines, including:

1. Mixing and ignition of fuel and air in the short residence times of a supersonic combustor.
2. The high heat loads and friction losses that occur at hypersonic speeds.
3. The control of thermal choking.
4. Non-equilibrium nozzle flows and the loss of energy from the cycle due to incomplete combustion.

Current day scramjet designers grapple with these same issues, although we now have 40 years of experience to guide us. Three further critical issues for practical hypersonic propulsion using scramjets are:

5. No thrust production below a flight Mach number ranging from 3.5-5, depending on the particular engine design. A booster or low-speed propulsion system is therefore required to raise the vehicle to the scramjet take-over Mach number.
6. Operating over a large Mach number range with a 'realistic' engine structure requires some finesse and many compromises for adequate performance at the upper and lower limits of the desired speed range.
7. The need for airframe integration.

The reason for (5) is straight forward; an engine that relies on shock compression in the inlet requires supersonic inflow, and further, if supersonic flow needs to be maintained in the combustor, this raises the lower limit for positive net thrust production even higher.

The reasons for (6) becomes abundantly clear as soon as scramjet performance calculations are attempted at different flight Mach numbers. At lower speeds where the stoichiometric heat of combustion is relatively large compared to the kinetic energy of the airflow, combusting fuel can produce large pressure rises in constant area combustors and possible choking or disruption to the flow through the engine, known as an unstart. Divergent combustors and/or step increases in combustor area are needed to allow fuel to react with a respectable proportion of the air captured by the engine in this instance. At higher speeds, however, where the kinetic energy of the airflow is significantly higher, combustor divergence can lead to chemical kinetics issues and incomplete combustion. Inlet contraction ratio requirements also change significantly with Mach number. Creating an engine that can operate over a large Mach number range is one of the key technological challenges in current times.

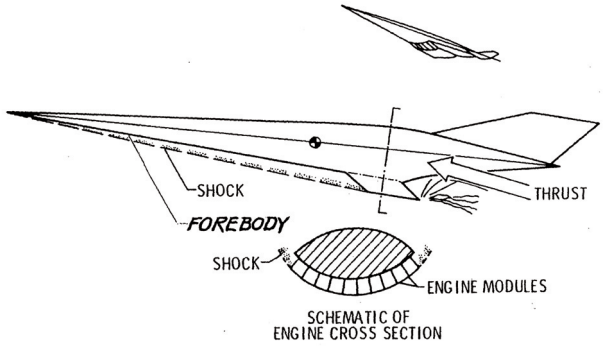

Figure 4. Airframe integrated scramjet powered vehicle (NASA).

A significant amount of research was conducted at NASA during the 1960s on axisymmetric pod-type scramjet engines, culminating in the Hypersonic Research Engine (HRE) Program. While this program demonstrated the validity of supersonic combustion and generated reasonable internal thrust levels at Mach 5, 6 and 7 (Andrews and Mackley 1994), the external drag of a pod-type configuration could not be overcome. It was realised that issue (7), the need for significant integration of the scramjet engine with the vehicle, was critical to the success of hypersonic airbreathing propulsion. Figure 4 shows a schematic of an airframe integrated scramjet powered vehicle, in which the vehicle forebody performs a portion of the engine compression and the vehicle aft-body forms part of the engine nozzle. Most current engine/vehicle concepts are variations on this theme, and this was the basic architecture for the National Aerospace Plane (NASP) Program in the United States.

The NASP Program was an aggressive effort initiated in 1985 by the Defense Advanced Research Projects Agency (DARPA) with the goal of developing a single-stage-to-orbit (SSTO) airplane called the X-30 (Barthelemy 1989). This vehicle was envisioned to take-off horizontally under gas-turbine power, accelerate to low earth orbit insertion velocity (7·9km/s) through the use of hydrogen-fuelled scramjets and rockets, and then return to earth for horizontal landing. It really was a 'space-plane' which would have brought aircraft-like operational flexibility to space. At the time of its demise in 1995 the NASP Program had not produced its goal of a working X-30 aircraft, however, it had spurred the development of many technologies related to hypersonics, including computational fluid dynamics (CFD), high temperature materials, and light-weight aerospace structures. It was also the genesis for the Hyper-X scramjet flight Program. Most current concepts for air-breathing access-to-space have moved away from NASP-like SSTO systems, and make use of the significant advantages of staging.

This article supplies a current status on the technological development of scramjets, as well as a description of current performance prediction methods. The stream thrust based cycle analysis methods used to calculate scramjet performance are presented first, including a description of the compression, combustion and expansion components that make up a scramjet and the key design issues for each. Two recent scramjet flight programs are then reviewed as examples of how sub-scaled scramjet flight tests are now being used as a step towards full-scale scramjet development. The article closes with a discussion of three-dimensional scramjet flowpaths and the reasons for the current resurgence in their study.

2.0 SCRAMJET PERFORMANCE ANALYSIS

The performance of a scramjet engine, either uninstalled or when integrated on a hypersonic vehicle, is most easily determined by what is called stream thrust analysis. This technique conserves the fluxes of mass, momentum and energy on strategically placed

https://doi.org/10.1017/S0001924000004796 Published online by Cambridge University Press

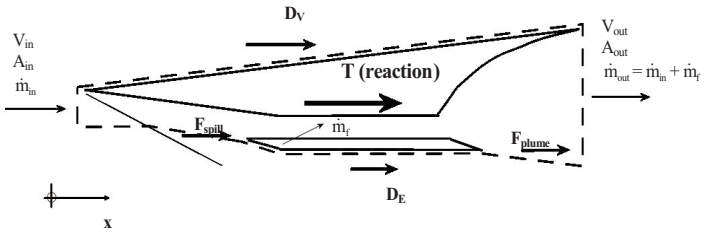

Figure 5. Schematic of control volume used for scramjet performance analysis.

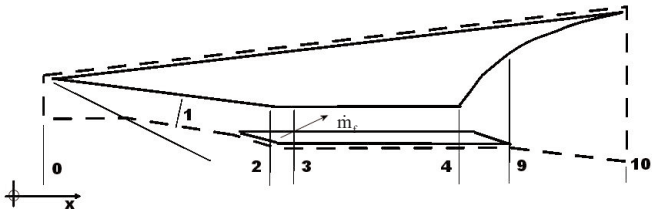

Figure 6. Flow stations for engine analysis.

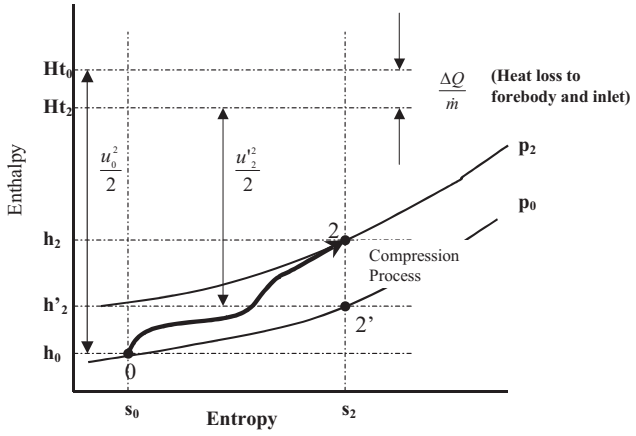

Figure 7. Mollier diagram of inlet compression process.

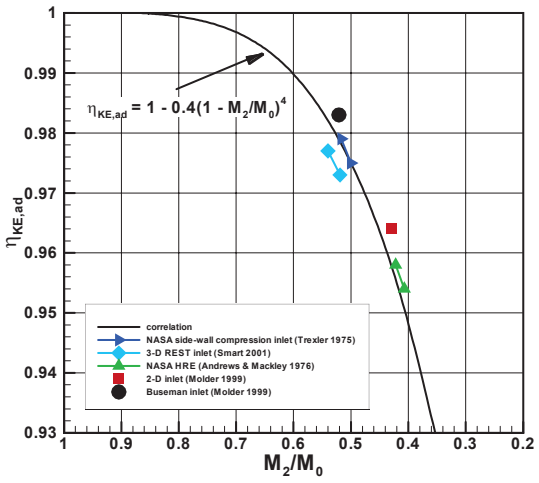

Figure 8. Inlet efficiency data.

control volumes to determine the propulsive forces on the vehicle. Figure 5 shows a schematic of a control volume that moves with and surrounds a hypersonic vehicle powered by a scramjet engine. Airflow enters the control volume at the flight conditions, fuel is added to the air in the combustor and the flow exits through the vehicle nozzle. For ease of analysis, the flow exiting the control volume is usually represented by a flux-conserved one-dimensional average of the real non-uniform exhaust plume. Only the axial forces will be considered here, however, similar relations can be developed for the transverse direction to determine the lift forces generated by the propulsion system.

For steady state flow through the control volume of Fig. 5, Newtons 2nd Law can be used to equate the summation of the forces on the control volume with the momentum flux across its surface. The summation of the axial forces on the control volume is as follows:

$$\sum F_{x_{CV}} = T + D_V + D_E + F_{spill} + F_{plume} + p_{in} A_{in} - p_{out} A_{out} \quad \ldots (1)$$

where the reaction force T is equal and opposite to the thrust generated by the vehicle, D_V is the drag of the vehicle, D_E is the external drag of the engine, F_{spill} is the spillage drag and F_{plume} is the drag associated with the expanding nozzle plume.

Equating these forces to the flux of momentum across the surface of the control volume yields the following relation:

$$T + D_V + D_E + F_{spill} + F_{plume} + p_{in} A_{in} - p_{out} A_{out} = \left(\dot{m}_f + \dot{m}_{in}\right) V_{out} - \dot{m}_{in} V_{in}$$

Rearranging and combining the spillage and plume drag into a single force called the additive drag (F_{add}) yields an expression for the thrust of the vehicle:

$$T = p_{out} A_{out} + \left(\dot{m}_f + \dot{m}_{in}\right) V_{out} - p_{in} A_{in} - \dot{m}_{in} V_{in} - D_v - D_{ex} - F_{add} \quad \ldots (2)$$

Using the definition of stream thrust, $F = pA + \dot{m}V$, we can express Equation (2) as:

$$T = F_{out} - F_{in} - D_v - D_{ex} - F_{add} \quad \ldots (3)$$

It is customary to separate the drag forces associated with the external aerodynamics of the vehicle and the engine from the internal operation of the engine. This is done through the definition of the uninstalled thrust of the engine, F_{un}, as follows,

$$T = F_{un} - D_v - D_{ex}$$

resulting in the following expression:

$$F_{un} = F_{out} - F_{in} - F_{add} \quad \ldots (4)$$

While it is more typical at lower speeds to account F_{add} to the vehicle along with the external drag forces, for scramjet applications F_{add} can have a relatively large magnitude, and it is considered more useful to make the propulsion system responsible for it.

Equation (4) indicates that the uninstalled thrust of an engine can be determined with knowledge of the stream thrust of the air entering the engine, the additive drag, and the stream thrust exiting the engine nozzle. The flow enters the engine at ambient conditions and at the flight velocity, so calculation of F_{in} reduces to a determination of the freestream capture area. Air spillage (and therefore spillage drag) decreases as the vehicle speed approaches the design point of the engine, and the plume drag varies depending on the amount of under-expansion in the nozzle. Both these forces are usually estimated through CFD analysis, or through rules-of-thumb based on empirical or experimental databases. Determination of F_{out} requires an involved analysis that follows the air

https://doi.org/10.1017/S0001924000004796 Published online by Cambridge University Press

through the complete scramjet flowpath. Many authors have presented analyses to calculate F_{out} for complete scramjet flowpaths with differing levels of sophistication and accuracy (Heiser and Pratt 1994[12], Pandolfini 1986[23], Pinckney *et al* 2004[25], Auslender and Smart 2000[3]). The analysis presented here is in the form used by this author.

2.1 Scramjet component analyses

Figure 6 shows a schematic of the internal flowpath of an airframe-integrated scramjet with particular reference stations highlighted. In keeping with the convention of Heiser and Pratt (1994)[12], station 0 is in the freestream flow ahead of the vehicle, and a streamtube with area A_0 is captured and processed by the engine. Station 1 is downstream of the vehicle forebody shock and represents the properties of the flow that enters the inlet. Station 2 is at the inlet throat, which is usually the minimum area of the flowpath, and the length between stations 2 and 3 is referred to as the isolator. Station 3 represents the start of the combustor, and fuel and air is mixed and burned by the end of the combustor at station 4. The nozzle includes an internal expansion up to station 9, and an external expansion to station 10 at the end of the vehicle.

It is appropriate to break the analysis needed to determine the stream thrust of the flow exiting the vehicle, and therefore the uninstalled thrust of the engine, into the three processes that make up the engine cycle; i.e. those of compression, combustion and expansion. While the compression and combustion processes can be blurred for some operating conditions, this convention will be adhered to here.

2.1.1 Compression

Efficient combustion of fuel requires that air be supplied to the combustor at a suitable pressure, temperature and mass flow rate. For a scramjet traveling at speeds greater than Mach 5 and at altitudes in the flight corridor of Fig. 3, this requires significant compression and heating of the air. For an airframe-integrated scramjet, both the vehicle forebody and inlet share this task. A multitude of different forebody/inlet configurations have been developed by many researchers (Van Wie 2001[38]), each designed to generate a specified level of compression over a range of flight Mach numbers. The performance of such compression systems can be separated into two key parameters; (1) capability, or how much compression is performed, and (2) efficiency, or what level of flow losses does the forebody/inlet generate during the compression process. Meaningful discussions of inlet performance must include both parameters as, for example, a highly efficient inlet can be very easily designed if it is required to do little compression.

Performance analysis of scramjet inlets involves the determination of the flow conditions at the inlet throat (station 2 of Fig. 6). A common parameter used to quantify the efficiency of the forebody/inlet compression is the kinetic energy efficiency, η_{KE}. The usefulness of this parameter, compared to many others, is that it can be used for non-ideal gas processes, and that its value has been found to be relatively independent of flight Mach number for a particular class of inlets. The definition of η_{KE} is the ratio of the kinetic energy the compressed flow would achieve if it were expanded isentropically to freestream pressure, relative to the kinetic energy of the freestream, and is most easily described on a Mollier diagram (Fig. 7). Here the flow entering the engine is compressed from p_0 to p_2. During the compression there is heat loss to the forebody/inlet structure, and:

$$\eta_{KE} = \frac{1/2u'^{2}_{2}}{1/2u_0^{2}} = \frac{H_{t2} - h'_2}{H_{t0} - h_0} \quad \ldots (5)$$

In some instances the adiabatic kinetic efficiency, $\eta_{KE,\,ad}$ is used. This parameter does not account for heat loss to the structure, and is defined as:

$$\eta_{KE,ad} = \frac{H_{t0} - h'_2}{H_{t0} - h_0} \quad \ldots (6)$$

When conducting scramjet performance calculations, two common methods for determining the properties at the inlet throat are; (1) use an empirical relation for η_{KE} in combination with a number of other parameters, and (2) use CFD to perform a numerical simulation of the forebody/inlet flowfield. An empirical correlation for $\eta_{KE,\,ad}$ (Waltrup *et al* 1982) in terms of the ratio of throat Mach number to freestream Mach number, M_2/M_0, is as follows:

$$\eta_{KE,ad} = 1 - 0\cdot 4 \left\{1 - \frac{M_2}{M_0}\right\}^4 \quad \ldots (7)$$

This expression relates inlet efficiency to an inlet capability parameter, M_2/M_0, so it satisfies our requirement for being a useful relation. However, in order to determine flow properties at the inlet throat, a more typical inlet capability parameter such as the pressure ratio (p_2/p_0) or temperature ratio, (T_2/T_0) is set as a requirement, an average ratio of specific heats (γ_{av}) is chosen, and an amount of heat loss to the vehicle is specified. Figure 8 compares Equation (7) with a summary of reported $\eta_{KE,ad}$ values calculated from mass flow based total pressure recovery measurements for a range of inlet geometries. It appears that for first order accurate performance calculations, Equation (7) is a reasonable choice for modelling the efficiency of the scramjet compression process.

Since the mid-1990s, modern computers and CFD codes have developed to the point where the calculation of turbulent flows through hypersonic inlets can be performed on a routine basis. A more accurate model of the scramjet compression process for a particular configuration can therefore be obtained through multiple CFD calculations over the operational flight Mach number. An example of this is shown in Fig. 9, where the flux-conserved, one-dimensional averaged inlet throat properties and mass capture ratio are plotted for a 2D forebody/3D inlet combination based on CFD calculations over a range of inlet Mach numbers[34].

In the design of hypersonic inlets there are some key issues that must be addressed in order to arrive at a useful configuration. These are:

1. Inlet starting limits
2. boundary-layer separation limits
3. Minimisation of external drag
4. Performance at off-design Mach number

The process of establishing supersonic flow through the inlet, known as inlet starting, puts a significant constraint on the internal contraction ratio of hypersonic inlets. This can be overcome through variable geometry, however, the weight and complexity of such can significantly degrade the overall system performance of a scramjet engine. Figure 10 shows a plot of some experimental data on the self-starting internal contraction ratio limit of 2D and 3D inlet configurations, as well as a theoretical starting limit developed by Kantrowitz and Donaldson (1945)[15]. The key parameter for inlet self-starting is the Mach number at the plane of cowl closure, M_c. It can be seen from the experimental data in Fig. 10 that the starting limit of Kantrowitz and Donaldson (1945)[15] is relatively accurate for 2D inlet geometries, but is conservative for the 3D inlets shown. In general, the self-starting limits of particular inlet classes are determined through experimental testing, and become more restrictive as M_c decreases. Figure 10 also shows such a self-starting limit developed from the 3D inlet data shown.

The flow through any practical hypersonic inlet will be turbulent, and can be prone to boundary-layer separation due to shock interactions. While minor separation may be acceptable, large-scale boundary-layer separation can create blockage of the engine and inlet unstart. Inlet flows are therefore required to satisfy established boundary-layer separation limits (Korkegi 1975)[16].

https://doi.org/10.1017/S0001924000004796 Published online by Cambridge University Press

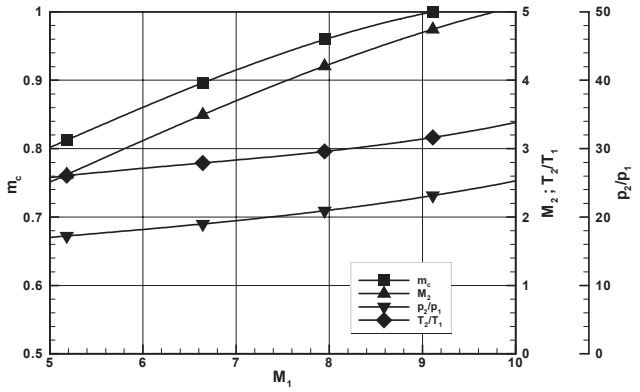

Figure 9 – CFD based Inlet capability parameters for 2D forebody/3D inlet combination.

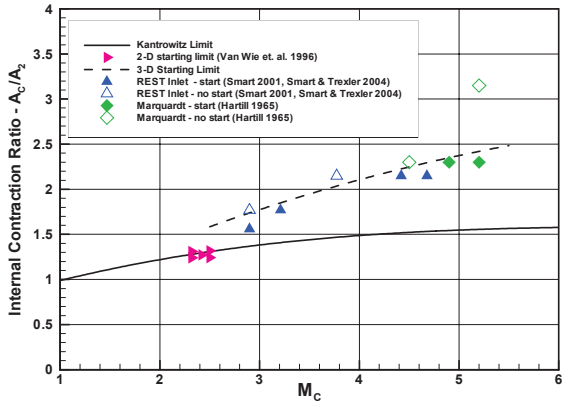

Figure 10. Experimental data on starting limits for 2D and 3D inlet geometries.

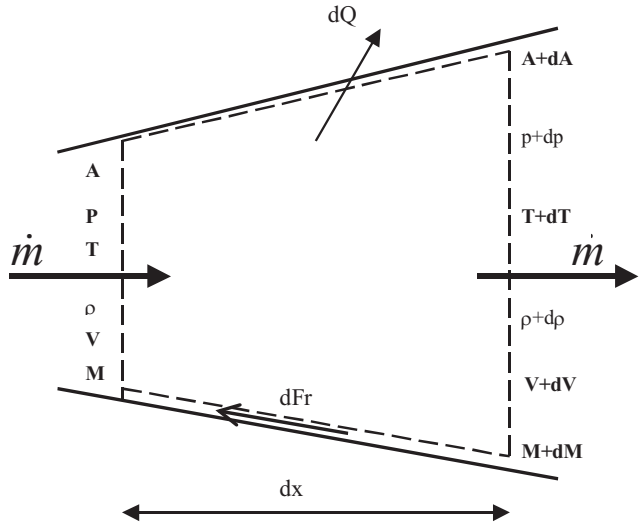

Figure 11. Differential element of combusting flow in a duct.

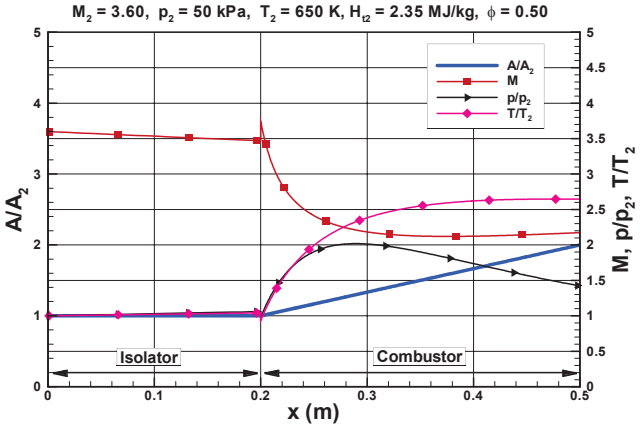

Figure 12. Attached flow through an isolator and divergent combustor.

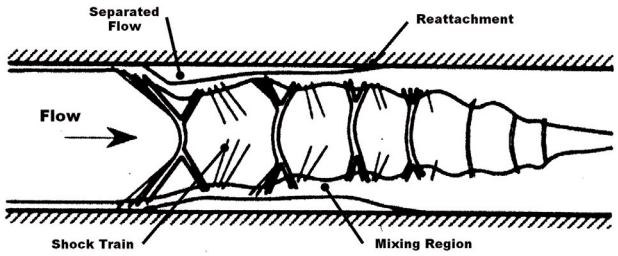

Figure 13. Flow model for separation in a duct.

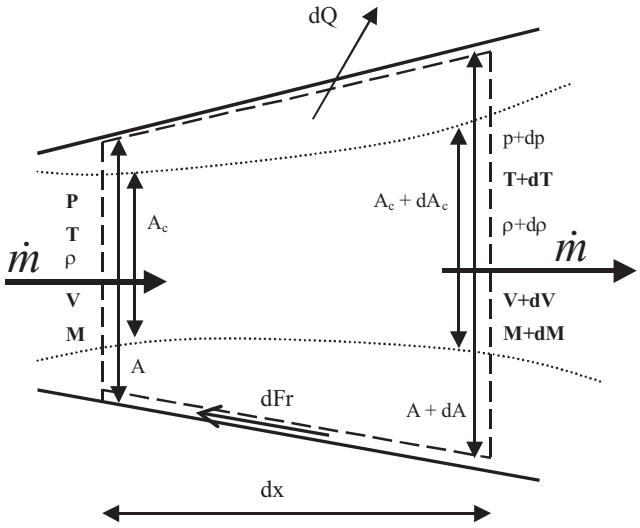

Figure 14. Differential element of separated flow.

https://doi.org/10.1017/S0001924000004796 Published online by Cambridge University Press

The minimisation of external drag is an important aspect of the inlet design process. The external drag on the inlet will always be an important parameter when comparing the performance of different engine configurations, and the minimisation of inlet external drag is one of the main drivers for airframe integration of scramjet engines. Finally, most inlet design methods are based on a particular design Mach number, usually at the upper limit of the operational Mach number range. Adequate off-design performance; i.e. at Mach numbers lower than the design point, is required, otherwise the vehicle will never reach it's design point.

2.1.2 Combustion

Analysis of the combustion process in a scramjet usually involves quasi-one-dimensional cycle analysis methods. While the real combusting flow in a scramjet is far from uniform at any cross-section throughout the engine, when used properly, these techniques provide an efficient means of modeling this region of a scramjet. While some methods simply jump from the start to the end of the combusting zone (Pandolfini 1986)[23], the method presented in this article enables prediction of the pressure distribution in the entire region of the engine affected by combustion, therefore enabling comparison with experimental data. These methods follow directly from the classical quasi-one-dimensional gasdynamics presented by Shapiro (1953)[29].

At flight speeds below Mach 8, combustion in a scramjet engine can generate a large local pressure rise and separation of the boundary layer on the surfaces of the combustion duct. This separation, which can feed upstream of the point of fuel injection, acts to further diffuse the core flow in the duct, and will interact with the inlet, possibly causing an unstart of the engine. A short length of duct, called the isolator, is usually added to the scramjet flowpath upstream of the combustor to contain this phenomenon. In some engines the combination of the diffusion in the isolator and heat release in the combustor decelerate the core flow to subsonic conditions, in what is called dual-mode combustion. At speeds above Mach 8, the increased kinetic energy of the airflow through the engine means that the combustion generated pressure rise is not strong enough to cause boundary-layer separation. Flow remains attached and supersonic throughout, and this is termed a pure scramjet. In this article, the quasi-one-dimensional analysis of pure scramjet flows is presented first, followed by analysis with the added complexity needed to deal with separated or dual-mode combustion flows.

A differential element of attached flow in a duct is shown in Fig. 11. Fuel and air are burning in this element, and a friction force $dF_r = \tau_w dA_W$ is applied by the walls, together with a heat loss in the amount dQ. For simplicity of analysis, the flow is assumed to be that of a calorically perfect gas with ratio of specific heats, γ, gas constant R, and constant pressure specific heat, c_p. Combustion heat release is modeled through the use of a heat of combustion, h_{pr}, and the change in total enthalpy of the flow as it traverses the element is:

$$dH_t = h_{pr} f_{st} d\phi - dQ$$

where f_{st} is the stoichiometric fraction of fuel to air, and $d\phi$ is the equivalence ratio of fuel that combusts in length dx.

The corresponding change in the total temperature of the flow is therefore $dT_t = dH_t/c_p$. The wall shear stress is related to a skin friction coefficient through $\tau_w = 1/2\rho V^2 C_f$, and $dA_w = 4Adx/D$, where D is the hydraulic diameter of the duct. The differential conservation equations of mass, momentum and energy for the element, are therefore given by:

$$\frac{d\rho}{\rho} + \frac{dV}{V} + \frac{dA}{A} = 0 \qquad \ldots (8)$$

$$\frac{dp}{p} + \frac{\gamma \mathrm{M}^2}{2}\frac{4C_f dx}{D} + \frac{\gamma \mathrm{M}^2}{2}\frac{dV^2}{V^2} = 0 \qquad \ldots (9)$$

$$\frac{dT}{T} + \frac{\gamma - 1}{2}\mathrm{M}^2\frac{dV^2}{V^2} = \left(1 + \frac{\gamma - 1}{2}\mathrm{M}^2\right)\frac{dT_t}{T_t} \qquad \ldots (10)$$

Together with the equation of state for the gas and the definition of Mach number (in differential form):

$$\frac{dp}{p} - \frac{d\rho}{\rho} - \frac{dT}{T} = 0 \qquad \ldots (11)$$

$$\frac{d\mathrm{Mv}^2}{\mathrm{M}^2} - \frac{dV^2}{V^2} + \frac{dT}{T} = 0 \qquad \ldots (12)$$

we have five equations to relate the seven variables. Following Shapiro (1953)[29], area change (dA/A) and total temperature change (dT_t/T_t) are treated as independent variables, and differential relations for all the other variables can be determined by elimination. The relation for Mach number is:

$$\frac{d(\mathrm{M}^2)}{\mathrm{M}^2} = \frac{-2\left(1 + \frac{\gamma - 1}{2}\mathrm{M}^2\right)}{1 - \mathrm{M}^2}\frac{dA}{A} + \frac{\left(1 + \gamma \mathrm{M}^2\right)\left(1 + \frac{\gamma - 1}{2}\mathrm{M}^2\right)}{1 - \mathrm{M}^2}\frac{dT_t}{T_t} + \frac{\gamma \mathrm{M}^2\left(1 + \frac{\gamma - 1}{2}\mathrm{M}^2\right)}{1 - \mathrm{M}^2}4C_f\frac{dx}{D} \qquad \ldots (13)$$

This relation may be integrated to determine the axial distribution of Mach number in ducts with specified area and a prior knowledge of the distribution of total temperature and C_f along the duct.

An example of the use of this methodology is plotted in Fig. 12, which shows the properties in a round combustor duct with an initial diameter of 60mm and a divergence with area ratio of 2. In this instance the properties at the throat (x_2 = 0·0m) are defined (M_2 = 3·60, p_2 = 50kPa, T_2 = 650K, H_{t2} = 2·35MJ/kg) and hydrogen fuel (h_{pr} = 119,954kJ/kg) is injected at x_3 = 0·2m with an equivalence ration of ϕ = 0·50. The amount of fuel that is allowed to react with the air at a particular station is dictated by a mixing efficiency curve, $\eta_m(X)$, that takes the form:

$$\eta_m = \eta_{m,e}\left[\frac{\vartheta \mathrm{X}}{1 + (\vartheta - 1)\mathrm{X}}\right] \qquad \ldots (14)$$

where $\eta_{m,e}$ is the mixing efficiency at the end of the combustor, $X = (x - x_3)/(x_4 - x_3)$ and ϑ is an empirical constant of order 1 to 10 which depends of the rate of mixing (Heiser and Pratt 1994)[12].

For the current example, $\eta_{m,e}$ was set to 0·8 and a value of ϑ = 5·0 was used. The heat release curve was therefore:

$$H_t = H_{t2} + h_{pr} f_{st} \phi \eta_m - dQ \qquad \ldots (15)$$

Skin friction was calculated based on a C_f = 0·002 and heat loss to the structure (dQ) was calculated using Reynolds analogy.

Given the limitation of constant γ, R and c_p in the analysis, Equation (13) is integrated in sections along the duct. In the isolator section upstream of fuel injection, values of γ = 1·37, R = 287J/kg/K and c_p = 1,063J/kg/K were used. In the combustor, average values of γ = 1·31, R = 297J/kg/K and c_p = 1,255/kg/K were used, so as to model the properties of the real fuel/air/combustion products mixture which vary along the length of the combustor. In the isolator section of the duct the Mach number reduces and the pressure and temperature increase due to the action of friction on the duct surfaces. At the start of the combustor, flow properties are recalculated to be consistent with the values of γ and R used in the combustor integration, while

https://doi.org/10.1017/S0001924000004796 Published online by Cambridge University Press

conserving fluxes of mass, momentum and total enthalpy across the boundary between the isolator and combustor. Fuel is also added, and combustion along the duct leads to a drop in the Mach number, an increase in the temperature, and the pressure varies smoothly in response to the competing effects of combustion and area increase. The peak pressure and temperature in the duct are p/p_2 = 2·02 and T/T_2 = 2·65, and the minimum Mach number is M = 2·12. The analysis results in an estimate of the one-dimensional properties of the flow as it exits the combustor at x_4 = 0·5m.

For the situation where flow separation occurs in the combustion region, the preceding analysis does not provide a useful model of the real flow, as the area of the core flow, A_c, is less than the geometric area. The core flow area represents a new variable, hence an extra relation is needed to close the problem. Figure 13 shows a sketch of a supersonic duct flow that has been separated by either combustion or some other imposed back-pressure, forming a 'pseudo shock' or 'shock-train' (Matsuo *et al* 1999)[17]. This phenomenon is characterised by a region of separated flow next to the wall, together with a supersonic core that experiences a pressure gradient due to the area restriction of the separation, forming a series of crossing oblique shocks in the core flow. A mixing region also grows between the core and separated flows, balancing the pressure rise in the core against the shear stress on the boundary of the separation. Finally, the flow reattaches at some point and mixes out to conditions that match the imposed back-pressure. It has been postulated by many authors that the pressure gradient in the core flow must be equal to the pressure gradient that can be supported by shear in the separated region. Based on a large amount of experimental data at different Mach numbers, Reynolds numbers and duct geometries, the pressure ratio p/p_i over a length dx was determined by Ortwerth (2001)[22] to vary as:

$$\frac{d\left(p/p_i\right)}{dx} = 4K\gamma\left(p/p_i\right)\mathrm{M}^2 \qquad \ldots (16)$$

where 4K = 44·5C_{f0} and C_{f0} is the friction coefficient at the initial separation point.

In essence, this relationship supplies the length scale required to achieve the full imposed pressure rise.

A differential element of the separated flow in a duct is shown in Fig. 14. The main difference between this and Fig. 11 is that the core area (A_c) is less than the geometric area (A). The conservation equations all relate to the core area, but friction and heat loss are based on the geometric area. In this instance, the energy equation, equation of state and definition of Mach number are the same as for the attached flow, but the mass conservation and momentum equations are now:

$$\frac{d\rho}{\rho} + \frac{dV}{V} + \frac{dA_c}{A_c} = 0 \qquad \ldots (17)$$

$$\frac{dp}{p} + \frac{\gamma\mathrm{M}^2}{2}\frac{4C_f dx}{D} + \frac{\gamma\mathrm{M}^2}{2}\frac{A_c}{A}\frac{dV^2}{V^2} = 0 \qquad \ldots (18)$$

Equation (16) is the extra relation required to close the separated flow problem. After a significant amount of algebraic manipulation, a relation for Mach number equivalent to Equation (13) is as follows:

$$\frac{d(\mathrm{M}^2)}{\mathrm{M}^2} = -\left(1+\frac{\gamma-1}{2}\mathrm{M}^2\right)\left[\frac{dp/p}{\frac{\gamma\mathrm{M}^2}{2}\frac{A_c}{A}} + \frac{4C_f\frac{dx}{D}}{\frac{A_c}{A}} + \frac{dT_t}{T_t}\right] \qquad \ldots (19)$$

This must be integrated in conjunction with the following relation for A_c/A:

$$\frac{dp}{p} + \frac{\gamma\mathrm{M}^2}{2}\frac{4C_f dx}{D} + \frac{\gamma\mathrm{M}^2}{2}\frac{A_c}{A}\frac{dV^2}{V^2} = 0 \qquad \ldots (20)$$

An example of the use of this methodology is plotted in Fig. 15, which shows the properties in the same round combustor duct as Fig. 12, but with reduced inflow Mach number and increased fuel equivalence ratio. In this instance the properties at the throat are M_2 = 2·65, p_2 = 50kPa, T_2 = 650K and H_{f2} = 1·59MJ/kg. Hydrogen fuel is injected at x_3 = 0·2m once again, and is assumed to combust with the same mixing curve as before (Equation (14)), but with an increased equivalence ratio of ϕ = 0·81. The same values of γ, R and c_p were also used for the isolator and the combustor. At these conditions the pressure rise from combustion separates the duct boundary layer (Korkegi 1975)[16]. The position at which separation occurs is iteratively chosen such that the flow may re-attach smoothly in the divergent section. Furthermore, if the core flow reduces to subsonic conditions in the separated region (as in this case), the flow must re-attach subsonically and then re-accelerate through a thermal throat at an axial position that can be calculated a priori, as outlined in Shapiro (1953)[29].

Figure 15 shows that the separation point that satisfies this criterion is at x = 0·988m. The core flow begins diffusing at this point at a rate dictated by Equation (16), reaching a minimum area of A_c/A_2 = 0·616. Combustion of fuel acts to push the flow towards re-attachment, which occurs at x = 0·284m with M = 0·961. The flow then re-accelerates through a thermal throat at x = 0·295m. Note that in comparison with the attached flow example (Fig. 12), the pressure and temperature rise in this dual-mode combustion flow are considerably higher, peaking at p/p_2 = 4·24 and T/T_2 = 3·64. While it is recognised that this analysis involves the significant assumption of a perfect gas, it does however contain all the physical attributes that are exhibited by real flows. Similar analyses of combustion flows using finite volume techniques and equilibrium chemistry are presented in Auslender and Smart (2000)[3].

In the design of scramjet combustors there are some key issues that must be addressed in order to arrive at a useful configuration. These are:

1. Adequate mixing of fuel and air
2. Fuel ignition and flame holding
3. Operation over a range of inflow conditions

The perennial issue of fuel/air mixing can never be ignored in the design of a scramjet, and this issue becomes more difficult as the flight Mach number increases. Consequently, a multitude of fuel injection/mixing schemes have been examined by a multitude of researchers over many years. These generally fall into three main categories; (1) strut based schemes, (2) flush wall injection, and (3) injection from ramps or bumps. Strut based schemes have high mixing rates through fuel addition in the middle of the combustor duct, but pay for this by creating a large disturbance to the flow. Strut cooling requirements and strong shock interactions are significant drawbacks of these systems, however they are sometimes utilised at the lower end of the scramjet flight envelope (Beckel *et al* 2006)[5]. Flush wall injectors create no physical blockage in the combustor, but suffer from long mixing lengths (Portz and Segal 2006)[26]. Ramp injectors attempt to reduce the flow blockage of struts, while still adding the fuel away from the combustor wall and thereby reducing fuel/air mixing lengths relative to flush wall injectors. Many geometries have been examined, (Donahue and McDaniel 1996)[9], most with streamwise fuel injection to take advantage of the thrust available from fuel injection. Flush wall and ramp injection schemes can be utilised over the full range of scramjet operation.

A fuel-air mixing model developed at NASA Langley Research Center (Northam *et al* 1991)[20] predicts the mixing distribution of a series of flush wall sonic injection holes on both sides of a two-dimensional combustor. The spacing between the fuel injectors for this configuration was equal to the gap height between the walls, G, and the fuel injector diameter was $d = G/15$. At an equivalence ratio of unity, the length required for complete mixing for this configuration is $x_L = 60G$, and the variation of mixing efficiency is given by:

$$\eta_m = 1\cdot01 + 0\cdot176\ln\left(\frac{x}{x_L}\right) \qquad \ldots (21)$$

https://doi.org/10.1017/S0001924000004796 Published online by Cambridge University Press

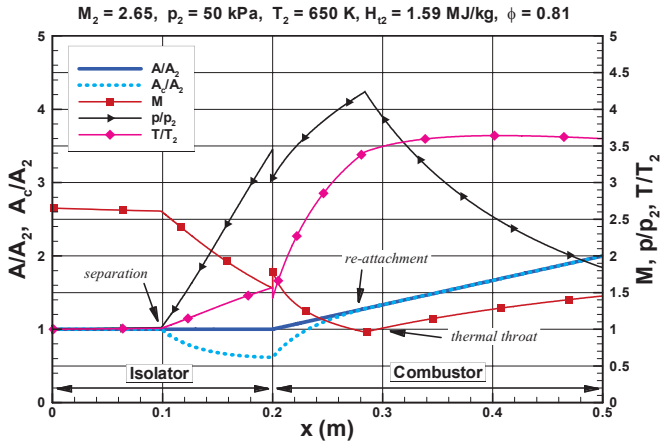

Figure 15. Thermally throated, separated flow through a divergent duct.

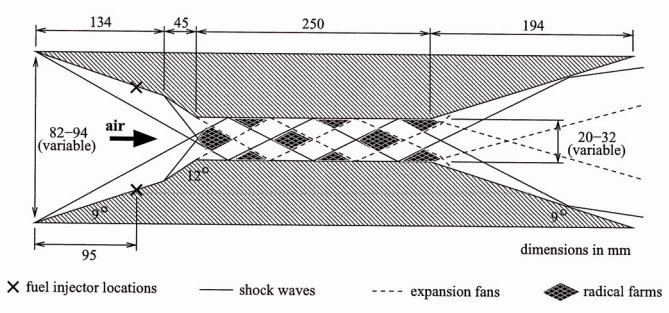

Figure 16. schematic of radical farming process.

Based on Equation (21), a mixing efficiency of 80% requires a length of 18·20G, which is an indication of the long mixing length typical of flush wall injectors.

Fuel ignition and flame holding are of course related to fuel mixing. Fuel injection schemes must not only generate fuel/air mixing, but also enable ignition of fuel, followed by stablisation of a combustion flame. At lower flight Mach numbers ignition aids such as spark plugs and highly reactive fuel additives are used to overcome ignition problems, although fuel additives can affect the specific impulse of the engine if these are required on a continuous basis. Physical flame holding regions such as steps and cavities are also utilised in some instances (Baurle and Eklund 2002)[6]. A recently developed technique for promoting ignition of fuel-air mixtures is called 'radical farming' (Odam 2004)[21]. For this technique the shocks in the inlet are arranged to form local regions of elevated pressure and temperature in the combustor, as indicated in Fig. 16. In the regions near the entrance of the combustor production of chemical radicals is encouraged. These 'radical farms' are terminated by the expansion waves from the corner at the combustion duct entrance, but the radicals remain 'frozen' in the flow until they meet another region of elevated temperature and pressure, where combustion continues. The benefit of radical farming is that, because of the exponential dependence on temperature of the rate of radical formation, the regions of elevated temperature and pressure in the radical farms provide accelerated development of the ignition process. It has been shown that this technique enables robust ignition of fuel at low inlet compression ratio's without the use of physical flame-holders (Odam 2004)[21].

In many instances it is desirable to operate a scramjet over a range of flight conditions, resulting in flow entering the combustor at a range of inflow conditions. If an engine is to operate in both dual-mode and pure scramjet mode, for example, then the engine configuration must be a hybrid design that allows scramjet mode transition. Fuel scheduling from multiple injection sites is often used in hybrid engines to increase the operational range of the combustor.

2.1.3 Expansion

The expansion process converts the potential energy of the combusting flow to kinetic energy and then thrust. In an airframe-integrated scramjet this begins in the divergent sections of the combustor and internal nozzle, and continues over a large portion of the vehicle aftbody. The shape of the aftbody also determines the direction of the gross thrust vector relative to the vehicles flight direction. An ideal

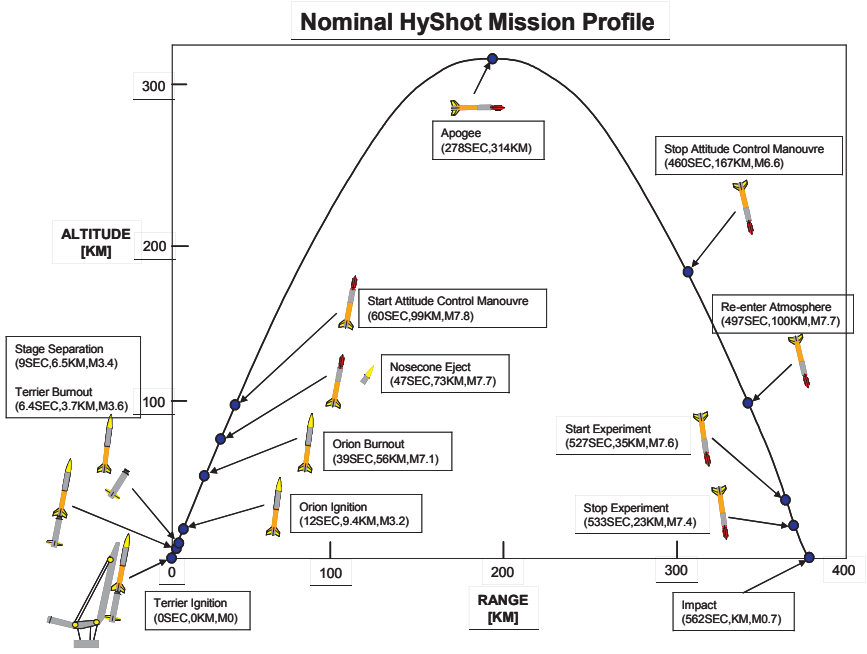

Figure 17. HyShot flight profile.

https://doi.org/10.1017/S0001924000004796 Published online by Cambridge University Press

Figure 18. HyShot 2 flight payload.

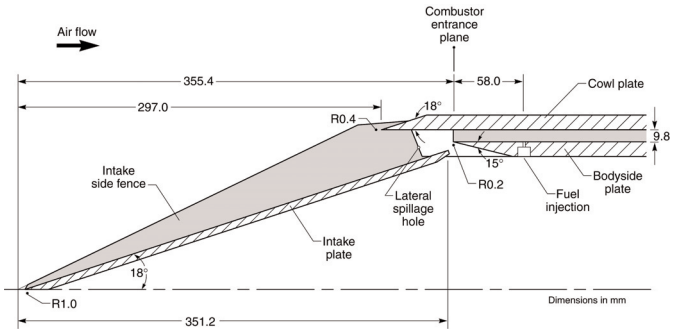

Figure 19. Schematic of the fuelled HyShot 2 flowpath.

expansion nozzle would expand the engine plume isentropically to the freestream pressure while it remains in chemical equilibrium, and this is the usual criterion that real nozzle flows are measured against. Loss mechanisms in practical expansion processes are due to:

1. Under-expansion
2. Failure to recombine dissociated species
3. Flow angularity
4. Viscous losses

The weight of a fully-expanding internal nozzle/aftbody would be prohibitive for most hypersonic vehicles, hence under-expansion losses are usually traded against vehicle structural weight. Dissociation losses result from chemical freezing in the rapid expansion process in the nozzle, essentially locking up energy that cannot be converted to thrust. This problem is exacerbated by inefficient compression, which leads to higher than necessary temperatures at the end of the combustion process. Flow angularity losses are a product of varying flow directions in the nozzle flow, and viscous losses are associated with friction on the internal nozzle and aftbody surfaces.

The aforementioned expansion losses are typically modelled using a nozzle efficiency parameter, η_N, which is applied as a gross thrust coefficient to the ideal stream thrust increment between the end of the combustor (station 4) and the end of the vehicle (station 10). The ideal stream thrust increment is calculated by isentropically expanding the flow at station 4 assuming chemical equilibrium to either, (1) a specified area based on an estimate of the size of the expanded plume, or (2) a specified pressure greater than or equal to the freestream pressure. Typical values for nozzle efficiency in this instance range between η_N = 0·85-0·95. At the completion of this expansion analysis, an estimate of the 1D properties at the vehicle exit is obtained (station 10) and following Equation 4, an estimate of the uninstalled thrust of a scramjet can be calculated.

It would be fair to say that the design of nozzle expansion systems for airframe-integrated scramjet vehicles is one of the least mature aspects of the overall design process. This may be due to the historical separation of the propulsion and airframe, with neither group wanting to take full responsibility for the engine nozzle/vehicle aftbody, where strong airframe-integration is necessary. This difficulty is exacerbated by the fact that the character of the engine plume can vary greatly with flight Mach number and engine throttle level. The engine plume can also affect the performance of vehicle trim surfaces and flaps. Despite this, confidence that these issues can be solved for practical vehicles was significantly increased by the recent successful flights of NASA's Hyper-X vehicle.

3.0 RECENT SCRAMJET FLIGHT PROGRAMS

Scramjet engine development has progressed to a current state where numerous flight tests have been conducted. These include the Australian HyShot 2, which flew at Mach 8 and was the first to demonstrate supersonic combustion in flight (July 2002); and NASA's Hyper-X vehicles, which successfully flew accelerating and cruise trajectories at Mach 6·9 (March 2004) and 9·6 (November 2004), respectively. Both these scramjet flight programs are reviewed here.

3.2 HyShot 2

The Centre for Hypersonics at The University of Queensland has routinely performed scramjet testing in shock tunnels since the early 1980s (Stalker *et al* 2006)[35]. Based on the desire to validate such testing for conditions in the Mach 7-8 regime, a sounding rocket based flight project known as HyShot was devised around 1997. This project involved two flight tests of a simplified supersonic combustion experiment designed solely through shock tunnel testing. While the HyShot scramjet payload was elegantly simple and quite robust, significant issues associated with providing suitable scramjet flight test conditions with the available rocket needed to be overcome. The chosen solution to these issues resulted in a highly parabolic trajectory, with the scramjet experiment being conducted during an almost vertical re-entry (Paull *et al* 2002)[24]. Following a first launch failure on 30 October 2001, the University of Queensland conducted a successful second launch on 30 July 2002.

Both HyShot flights took place at the Woomera prohibited area Test range in central Australia. Each used a two-stage Terrier-Orion Mk70 rocket that generated a highly parabolic trajectory to boost the payload and the exhausted second stage Orion motor to an apogee in excess of 300km, as shown in Fig. 17. This combination of rocket and trajectory allowed the payload and attached second stage to re-enter the atmosphere with a Mach number in excess of 7·5 at altitudes between 35 and 25km, thus supplying a range of conditions within the flight corridor of Fig. 3.

The HyShot payload included a nose-cone to shroud the scramjet flowpaths on the initial ascent, two scramjet combustors orientated back-to-back on a wedge forebody, plus hydrogen and nitrogen tanks, batteries, telemetry system, flight computer and other components. One combustor was hydrogen fuelled through 4 laterally spaced normal

https://doi.org/10.1017/S0001924000004796 Published online by Cambridge University Press

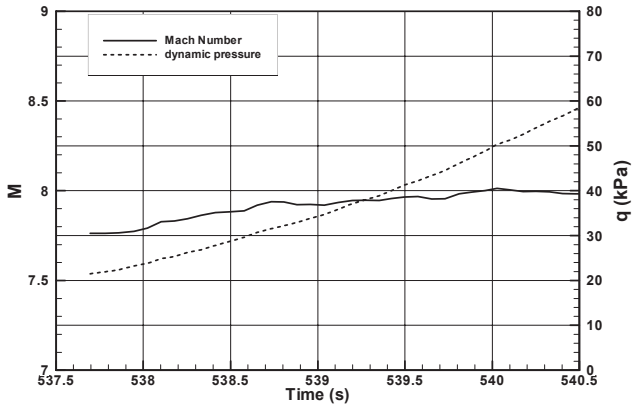

Figure 20. Reconstructed Mach number (M) and dynamic pressure (q) histories.

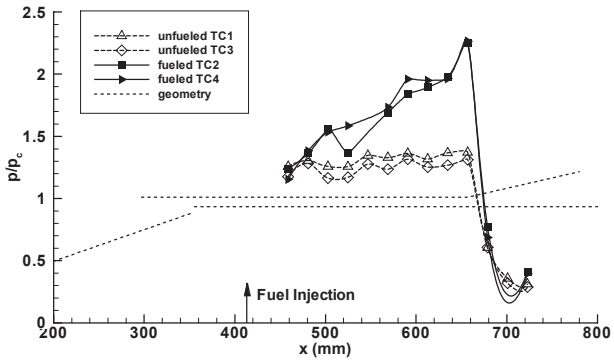

Figure 21. Windward fueled and un-fueled combustor pressure distributions (x = axial distance from nose of payload).

injectors, while the other combustor was unfuelled so as to obtain baseline (tare) conditions to compare against the fuelled flowpath throughout the flight. Figure 18 shows a photograph of the payload used for HyShot 2 (with the shroud removed). It was constructed predominantly of copper alloy for rapid dissipation of aerodynamic and combustion generated heat loads, with TZM (tungsten-zirconium-molybdinum) used for the highest heat flux regions that occurred at the leading edges of both combustors.

The goal of the experiment was to supply uniform flow into the two rectangular combustors at conditions ranging between Mach 7·2 and 8·0, allowing for an angle-of-attack (α) variation of the payload between +5 and –5 degrees. Figure 19 shows a schematic of the fuelled flowpath. The intake consisted of a single 18°deg. wedge with a width of 100mm, a blunted leading edge, and highly swept side fences. The high wedge angle was necessary to ensure that the combustor entrance temperature and pressure were great enough to readily induce self-ignition of hydrogen. The rectangular combustor had a constant area 9·8mm x 75mm cross-section and a length of 300mm (length/height = 30·61). The combustor cowl spanned the full width of the intake wedge and was situated such that the intake shock was upstream of its leading edge at all times. The flowpath design incorporated a shock trap that was situated between the end of the intake wedge and the entrance of the combustor. This feature not only captured the cowl shock, but also bled off the intake boundary layer. The reduced width of the combustor (relative to the intake wedge) and lateral spillage holes in the side fences adjacent to the shock trap were designed to remove the fence boundary layers and corner flows.

Table 1
Flight parameters for analysed time slices

number	Time(s)	Flight Mach	Flight dynamic pressure (kPa)	Altitude (km)	angle-of -attack (degrees)
1	538·103	7·828	24·88	34·48	–5·012
2	538·179	7·831	25·33	34·31	5·540
3	538·734	7·938	31·55	33·05	–5·081
4	538·805	7·938	32·20	32·89	4·617

The flight produced a significant set of scramjet combustor data at varying duct entrance pressure, temperature and Mach number. Trajectory reconstruction was accomplished using onboard sensors alone (Cain *et al* 2004). Fuel flow was initiated at approximately t = 536·5 seconds after launch as the payload and attached Orion motor re-entered the atmosphere. Figure 20 shows the Mach number and dynamic pressure time histories during three seconds of the experimental window, and Table 1 lists four zero-yaw time slices used for analysis. Figure 21 shows a comparison of the fuelled and unfuelled combustion pressure distributions at windward conditions: i.e. when each duct was at a positive angle-of-attack of approximately 5 degrees. Note that all data are normalised by the combustor entrance pressure (p_c) in order to make meaningful comparisons. The equivalence ratio of the fuelled duct was approximately 0·34, and the pressure rise from combustion of the hydrogen fuel is clearly evident. Cycle analysis of this data indicated that supersonic combustion occurred at these times slices during the flight, at a combustion efficiency for the fuel of 81% (Smart *et al* 2006)[33,34].

While the motivation for the HyShot 1 and 2 flights was ostensibly to determine the differences between scramjet performance in a shock tunnel and flight, the real benefit of the program was learning how to fly at hypersonic speed in the atmosphere. Overcoming all the severe engineering challenges that this entailed has had a significant effect on the types of scramjet configurations that will be examined at the Centre for Hypersonics in the future. It is the view of this author and all the team involved with HyShot that flight-testing should be an integral part of any scramjet development program, and not just the final step in the development process. The success of the HyShot 2 flight has led to a significant interest in low cost scramjet flight-testing using sounding rocket boosters. Two further flights (HyShot 3 and 4) were conducted by The University of Queensland in March 2006, with further flights planned.

3.3 Hyper-X

The NASA Hyper-X Program conducted the most realistic flight tests of hypersonic airbreathing engines to date. Unlike HyShot 2, the Hyper-X flight vehicle separated from its booster to fly a controlled hypersonic trajectory under scramjet power. Two successful flights were conducted; the first at Mach 6·9 on 27 March 2004, and a second at Mach 9·6 on 16 November 2004. Both included 5+ seconds of hydrogen fuelled scramjet operation, followed by a series of hypersonic aerodynamic manoeuvres as the vehicle decelerated.

The Hyper-X vehicle, a schematic of which is shown in Fig. 22, had significant heritage from the NASP Program (Rausch *et al* 1997). It was a 'smart scaled' version of a 200ft operational vehicle, that could be flight tested within available budgets while also demonstrating operation of a dual-mode hydrogen fuelled scramjet. The chosen 12ft (3·65m) vehicle had a single airframe-integrated scramjet and was boosted to flight conditions using a modified Pegasus booster that was air-launched from a B-52 from Edwards AFB in California. The desired test conditions

https://doi.org/10.1017/S0001924000004796 Published online by Cambridge University Press

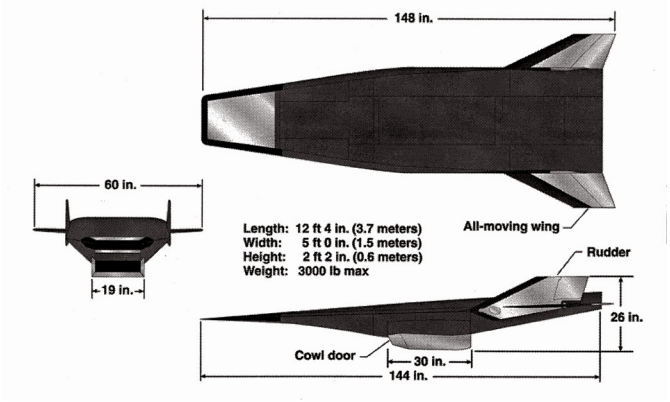

Figure 22. Hyper-X vehicle configuration (NASA).

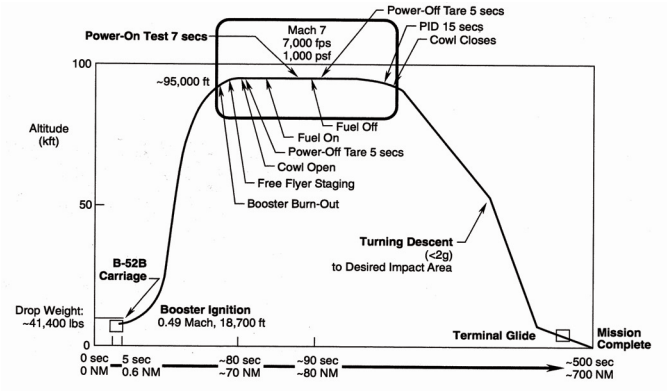

Figure 23. Nominal Mach 7 Hyper-X flight trajectory (NASA).

Figure 24. HXFE engine in 8-FT HTT with flow from right to left. (NASA).

were 95,000ft (~29·0km) at Mach 7, and 110,000ft (~33·5km) at Mach 10, both of which correspond to a dynamic pressure of 1,000psf (~48kPa) (Voland *et al* 1998). The flight sequence for the Mach 7 flight is shown in Fig. 23. The free-flying portion of the flight included separation from the booster, engine cowl opening, 5+ seconds of scramjet operation, fuel-off flight with the cowl open, and aerodynamic manoeuvres with the cowl closed. A similar sequence was conducted at Mach 10. The vehicles flown on the two flights were nominally of the same external shape, but had different thermal protection systems and different engine designs. Internal details of the scramjet flowpaths have not been released, however, the configurations were nominally two-dimensional with a rotating cowl for opening and closing the engine duct.

The Hyper-X vehicle enabled flight testing of a complete forebody, internal engine, and aftbody/thrust nozzle for the first time. The Mach 7 engine was developed through a long series of partial flowpath and subscale testing at NASA Langley Research Center, followed by a complete tip-to-tail flowpath simulation in the 8 foot High Temperature Tunnel (8-FT HTT), also at NASA Langley. A photograph of this engine, known as the Hyper-X Flight Engine (HXFE), is shown in Fig. 24. It was mounted upside down in the test section of the 8-FT HTT on a force balance with identical internal system components to those used in flight. The main objectives of this pre-flight testing were to validate the Mach 7 propulsion database and to verify the operation of system components. Not only were the engine operability and performance data acquired during testing, but realistic estimates of the aero-propulsive vehicle force and moment increments due to both opening the cowl door and combustion were obtained (Huebner *et al* 2001)[14]. The Mach 7 flight vehicle flew a flawless trajectory that showed positive net thrust during scramjet operation and engine pressure distributions very similar to those measured in the 8-FT HTT (Ferlemann *et al* 2005)[10].

While the Mach 7 engine was able to be ground tested in long duration facilities, only impulse facilities can generate conditions to simulate Mach 10 propulsive flight on the ground. The ground tests to support development of the Mach 10 engine were done at the NASA HyPulse shock tunnel (Rogers *et al*, 2005)[28]. This meant that only instantaneous testing was possible, and engine sequences such as piloting and fuel ramp-up could not be simulated. Despite this, the Mach 10 engine performed to expectation, reaching cruise conditions during scramjet operation (McClinton, 2006)[18].

The Hyper-X program involved the first flight tests of a complete scramjet powered vehicle. The key results derived from the two successful flights were:

1. Airframe integrated scramjet powered vehicles can fly stable, controlled trajectories at hypersonic speeds.
2. Accelerating hypersonic flight is possible at Mach 7 using air-breathing propulsion.
3. Hypersonic cruise is possible at Mach 10 with a non-optimised vehicle/engine combination.
4. Ground test experiments, CFD analysis and other aerodynamic tools can be used to design scramjet powered flight vehicles.

Charles McClinton, manager of the Hyper-X Program, summarised the results of the Program by stating that the flights provided an "*essential demonstration of the capability of hypersonic air-breathing vehicle design tools*", and that the "*technology advancements made by these flight tests could not have been made using just wind-tunnels and CFD*" (McClinton, 2006)[18].

4.0 THREE-DIMENSIONAL SCRAMJETS

The history of scramjet development has seen a progression from experiments to validate the existence of supersonic combustion, to simple axi-symmetric configurations that owed their 'pod-type' shape to gas turbine heritage, and then to airframe integrated engines with 2D inlets and rectangular combustors (such as Hyper-X). In recent times it has become clear that from an overall system perspective, a flowpath based on 2D geometry may not be optimum for high thrust/weight or robust fluid-dynamic performance of the engine. Scramjet flowpaths with elliptical or round combustors have therefore been studied (Smart and Ruf 2006[33]; Beckel *et al* 2006[5]). These engine concepts attempt to take advantage of:

1. The inherent structural efficiency of rounded shapes. This potentially enables reduced structural weight.
2. The reduced wetted area of elliptical cross-sections relative to rectangular shapes for the same cross-sectional or flow area. (Reduced wetted area lowers viscous drag and cooling requirements in the high dynamic pressure combustor environment.)
3. The removal of the potentially detrimental fluid dynamic effects of corner flows in scramjet isolators and combustors. This may improve the back-pressure limits of the inlet/isolator, or alternatively, reduce isolator length requirements.

https://doi.org/10.1017/S0001924000004796 Published online by Cambridge University Press

In order to integrate smoothly with the vehicle, scramjet flowpaths with 'rounded' combustors are inherently three-dimensional. Recent developments in these three-dimensional scramjets are reviewed here through application to both hypersonic cruise and access-to-space systems.

A key enabling technology for the use of elliptical combustors in airframe-integrated scramjets is the design of hypersonic inlets with 3D shape transition. For vehicles with essentially planar forebody shapes, the required transition is from a rectangular-like capture area to an elliptical isolator/combustor shape (noting that a circle is an ellipse with an aspect ratio of unity). A design process developed for these Rectangular-to-Elliptical Shape Transition (REST) inlets (Smart 1999) utilises a quasi-streamline-tracing technique to produce an inlet with highly swept leading edges, a cut back cowl, and the desired shape transition to an elliptical throat. The REST inlets resulting from these procedures have almost 100% mass capture at the design Mach number, and operate below the design Mach number by spilling air past the cut back cowl. An important aspect of this computationally intensive design procedure is the ability to reduce inlet length until shock wave/boundary-layer separation criteria are met.

Figure 25 shows a REST inlet model with a design point of $M_1 = 6{\cdot}0$ installed in the Arc Heated Scramjet Test Facility (AHSTF) at NASA Langley Research Center. This inlet was designed to be installed on a vehicle with a short 6° forebody, hence the flight design point was $M_0 = 7{\cdot}1$. Testing at $M_1 = 6{\cdot}2$ (Smart 2001)[31] showed that this inlet was highly efficient, and self-started with an internal contraction ratio well above the Kantrowitz limit (see Fig. 10). However, further testing in the same facility showed that this inlet would not start at $M_1 \sim 4{\cdot}7$ (see Fig. 10). In order for REST inlets to be an effective fixed-geometry configuration, it was recognised that they must self-start and have adequate performance at Mach numbers well below the design point. This led to some amendment of the design method to allow both a reduction in the internal contraction ratio and the installation of spillage 'gills'. Subsequent testing of an inlet with a design point of $M_1 = 5{\cdot}7$ using the adapted inlet design procedures showed robust starting, strong back-pressure resistance and good efficiency at $M_1 = 4{\cdot}0$ (Smart and Trexler 2004). Together with a significant amount of CFD analysis to examine internal flow variations at different Mach numbers, these tests indicated that REST inlets are a viable fixed-geometry configuration for airframe-integrated scramjets operating over a significant Mach envelope.

Fuel injection schemes for elliptical combustors are not expected to be significantly different from those utilised in rectangular combustors. At speeds below Mach 8 where dual-mode operation is required, flush wall injectors in combination with ramps, bumps, steps and cavities are the most likely candidates, whereas solutions such as radical farming can be adapted to 3D flowpaths for pure scramjet operation above Mach 8. In terms of structural strength and reduced wetted area, a round combustor is optimum. However, a round combustor shape is not ideal for the minimisation of fuel/air mixing length. Introduction of an elliptical shape with an aspect ratio in the range of two, for example, means that fuel injection from the longer sides need only penetrate half as far in order to reach the air in the central region of the combustor. In general, overall fuel/air mixing length will reduce with increased ellipse aspect-ratio, however the introduction of in-stream fuel injection elements can decouple mixing length from the combustor shape (Beckel *et al* 2006)[5]. In general, a compromise between structural weight/unit length and mixing length will determine the optimum combustor aspect ratio in an elliptical combustor scramjet.

Three-dimensional scramjets for hypersonic cruise applications have developed to the point that exploratory engine tests have been performed in the wind-tunnel. Testing of a REST Scramjet designed for flight within a Mach 4·5-8·0 envelope was conducted in 2005 at conditions well below the design point of Mach 7·1. These experiments were conducted in a combustion-heated facility at NASA Langley Research Center at a simulated flight Mach number of 5·3

Figure 25. REST inlet model installed in the AHSTF (NASA).

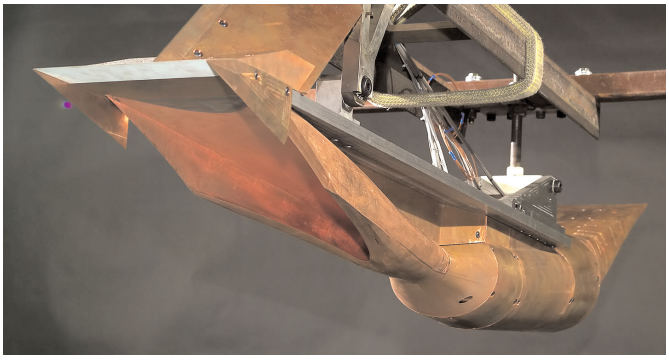

Figure 26. Mach 4·5-8·0 REST scramjet test article (NASA).

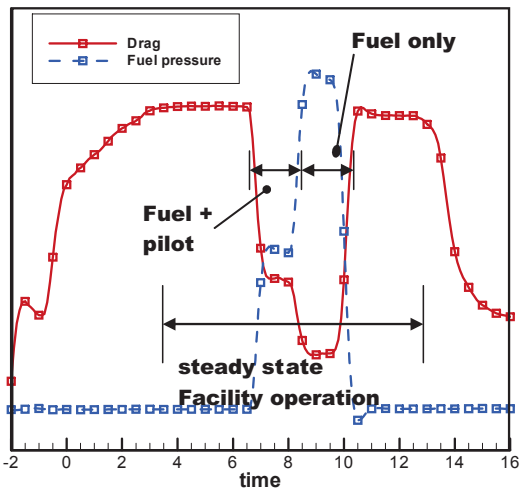

Figure 27. Time histories of drag force and fuel line pressure.

https://doi.org/10.1017/S0001924000004796 Published online by Cambridge University Press

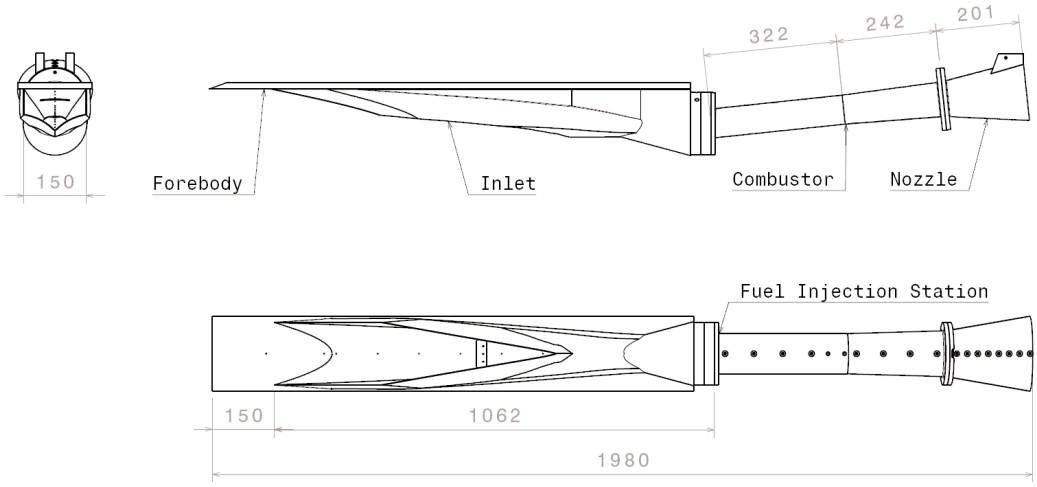

Figure 28. Schematic of the RESTM12 engine model (dimensions in mm).

(Smart and Ruf 2006)[33]. Figure 26 shows the fully assembled engine model prior to installation in the wind-tunnel. The test article, approximately 2 metres long and 0·2 metres wide, was of thick-walled copper construction for heat sink capability with a maximum test duration of 30 seconds. The engine model was comprised of four major components; (1) a REST inlet with a 12·7cm forebody plate, (2) an elliptical injector block, (3) a divergent elliptical combustor, and (4) a nozzle, which comprised of a fully enclosed internal section and an asymmetric external section which transitioned back to a rectangular shape for efficient vehicle integration. These four components were assembled end-to-end, and attached to a steel backing plate in a manner which allowed the engine to freely expand longitudinally during a test. The entire engine assembly was suspended in the facility test section on a 6-component force balance, and the engine was fuelled with room temperature gaseous hydrogen. At these lower flight enthalpies a pilot is often required to ignite the fuel and establish flame holding. In this instance a gaseous 20% silane – 80% hydrogen (molar basis) pyrophoric pilot was used.

The goals of the test program were two-fold: (1) to quantify the REST inlet performance and operability characteristics when incorporated within a complete engine flowpath; and (2) determine, for the first time, the overall performance attributes of this class of scramjet. Figure 27 shows time histories of the drag force measured by the force balance and the fuel supply pressure during a typical fuelled engine test. The facility reached steady state conditions at t = 4·0 seconds, at which time the drag force corresponded to a started flowpath with no fuel injection. At approximately t = 7·0 seconds the silane-hydrogen pilot and hydrogen fuel were turned on, producing a reduction in the measured drag force. At approximately t = 8·0 seconds the pilot flow was reduced to zero and the hydrogen flow was increased to its steady state value for the test, corresponding to an equivalence ratio of ϕ = 1·09. This produced a further reduction in the drag force to a level consistent with robust combustion within the engine. At approximately t = 10 seconds the hydrogen fuel valve was closed, and the facility began its shutdown procedure at t = 13·5 seconds.

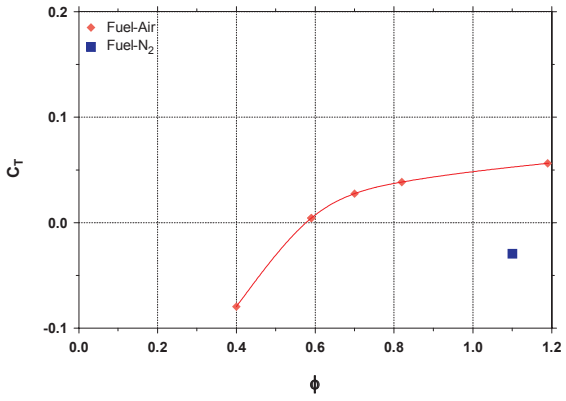

Figure 29. Thrust coefficient for combustor injection at ϕ = 0·4 – 1·2.

The major results of the test program were that the inlet self-started on all occasions and that testing with hydrogen fuel at equivalence ratio's between 0·5 and 1·5 exhibited robust combustion within the engine after the silane-hydrogen pilot was removed. These results indicate that the inlet/isolator combination utilised in the flowpath was adequate for operation near the lower end of the design Mach number envelope, and are considered optimistic for the use of this type of configuration for acceleration to hypersonic cruise at Mach 7-8. Testing of this model at the higher end of its design flight regime is planned in the near future.

A three-dimensional scramjet for access-to-space applications has recently undergone testing in the T4 shock tunnel at The University of Queensland. This flowpath is a REST configuration with a design flight envelope from Mach 6-12, and is a candidate engine for the airbreathing portion of a three-stage rocket-scramjet-rocket access-to-space system (Smart and Tetlow 2006)[34]. At the Mach 12 design point the engine operates as a pure scramjet, however in order to be effective at the lower end of its flight envelope, allowances have been made for dual-mode operation below Mach 7. As the generation of useful thrust levels above Mach 10 is the least well understood portion of the desired range, initial experiments were conducted at conditions equivalent to Mach 12 flight. A dimensioned schematic of the engine is shown in Fig. 28. The overall model was 1·98m long and consisted of a forebody plate, REST inlet, elliptical combustor, and a short elliptical nozzle with a final area ratio of 8·0 relative to the inlet throat. The capture area of the inlet was 0·15m wide and gaseous hydrogen fuel was injected in a streamwise direction from a small backward facing step at the start of the combustor through 48, 1·5mm diameter holes.

All tests of this engine completed to date have indicated robust combustion of fuel. Figure 29 shows a plot of thrust co-efficient against equivalence ratio for the experiments, indicating steady thrust increase with fuel level between ϕ = 0·4 and 0·7, followed by a tapering off of thrust increase due to mixing limitations. The thrust due to fuel injection into nitrogen is also shown in the figure, to indicate the clear effect of combustion. The thrust was calculated in this instance by integration of the pressure measurements in the combustor and nozzle, with the following terms subtracted; (*i*)

https://doi.org/10.1017/S0001924000004796 Published online by Cambridge University Press

internal inlet drag calculated using CFD and (*ii*) no-fuel viscous drag on the combustor and nozzle calculated using CFD. This methodology was considered to be best for arriving at a realistic value for thrust, however it does not include any skin friction reduction from boundary-layer combustion, which may be significant (Stalker 2005). These preliminary results are considered promising for the application of this type of engine for access-to-space. Future testing will include fuel injection in the inlet and experiments at lower equivalent flight Mach numbers.

5.0 CONCLUDING REMARKS

This article gives a brief overview of some recent scramjet developments in the context of historical scramjet programs over the last 50 years. It also supplies a description of current methods for determining the performance of both pure scramjet and dual-mode scramjet engines, and indicates how the results of recent scramjet flight programs have shown why sub-scale flight testing should be an integral part of any scramjet development program. The goal of single-stage-to-orbit craft with aircraft-like flexibility has receded into the future, however it has been replaced by nearer term applications like hypersonic cruise within the atmosphere and the airbreathing stage of a multi-stage access-to-space system. The resurgence of interest in three-dimensional configurations has been brought about by interest in these nearer-term applications, as well as the increased capability of computers and CFD software. While preliminary in nature, the three-dimensional scramjet studies described in this article indicate that three-dimensional flowpaths may be applicable to these nearer-term goals. It is possible that the next decade will be the period when long duration hypersonic flight within the atmosphere becomes a reality.

ACKNOWLEDGEMENT

I would like to acknowledge the inspirational achievements of Professor Ray Stalker and Mr Griffin Anderson throughout their long and distinguished careers.

REFERENCES

1. ANDERSON, G.Y., MCCLINTON, C.R. and WEIDNER, J.P. Scramjet Performance, *Scramjet Propulsion, Progress in Astronautics and Aeronautics*, 2001, AIAA, Washington DC, USA, Chapter 6.
2.. ANDREWS, E.H. and MACKLEY, E.A. Analysis of experimental results of the inlet for the NASA hypersonic research engine aerothermodynamic integration model, 1976, NASA TM X-3365.
3. AUSLENDER, A.H., and SMART, M.K. Comparison of Ramjet Isolator Performance with Emphasis on Non-Constant Area Processes, 2000, Joint Army-Navy-NASA-Air Force (JANNAF) Meeting, Monterey, California, USA.
4. BARTHELEMY, R.R. The national aero-space plane program, 1989, AIAA Paper 89-5001.
5. BECKEL, S.A., GARRETT, J.L. and GETTINGER, C.G. Technologies for robust and affordable scramjet propulsion, 2006, AIAA paper 2006-7980.
6. BAURLE, R.A. and EKLUND, D.R. Analysis of dual-mode hydrocarbon scramjet operation at Mach 4-6.5, *J Propulsion and Power*, 2002, **18**, (5), p 990.
7. CURRAN, E.T. Scramjet engines: The first forty years, *J Propulsion and Power*, 2001, **17**, (6), pp 1138-1148.
8. CAIN, T., OWENS, R. AND WALTON, C. Reconstruction of the HyShot 2 flight from onboard sensors fifth symposium on aerothermodynamics for space vehicles, 2004, Cologne, Germany.
9. DONOHUE, J.M. and MCDANIEL, J.C. Complete three-dimensional multi-parameter mapping of a supersonic ramp fuel injector flowfield, *AIAA J*, 1996, **34**, (3), p 455.
10. FERLEMANN, S.M., MCCLINTON, C.R., ROCK, K.E. and VOLAND, R.T. Hyper-X Mach 7 scramjet design, ground test and flight results, 2005, AIAA paper 2005-3322.
11. FERRI, A. Review of the problems in application of supersonic combustion, *Aeronaut J*, 1964, **64**, (645), pp 575-597.
12. HEISER, W.H. and PRATT, D.T. Hypersonic airbreathing propulsion, *AIAA Education Series*, 1994.
13. HENRY, J.R. and ANDERSON, G.Y. Design considerations for the airframe-integrated scramjet, 1973, NASA TM X-2895.
14. HUEBNER, L.D., ROCK, K.E., RUF, E.G., WITTE, D.W. and ANDREWS, E.H. Hyper-X flight engine ground testing for flight risk reduction, *J Spacecraft and Rockets*, 2001, **38**, (6), pp 844-852.
15. KANTROWITZ, A. and DONALDSON, C. Preliminary investigation of supersonic diffusers, NACA WRL-713, 1945.
16. KORKEGI, R.H. 1975, Comparison of shock induced two- and three-dimensional incipient turbulent separation, *AIAA J*, **13**, (4), pp 534-535.
17. MATSUO, K., MIYAZATO, Y. and KIM, H. Shock train and pseudo-shock phenomena in internal gas flows, *Progress in Aerospace Sciences*, 1999, **35**, pp 33-100.
18. MCCLINTON, C.R. X-43 – scramjet power breaks the hypersonic barrier: Dryden lectureship in research for 2006, 2006, AIAA paper 2006-1.
19. MOLDER, S. Performance of three hypersonic inlets, paper 1430, 22nd International Symposium on Shock Waves, 1999, London, UK.
20. NORTHAM, G.B., CAPRIOTTI, D.P., BYINGTON, C.S. and GREENBERG, I. Mach 2 and Mach 3 mixing and combustion in scramjets, AIAA paper 91-2394, 1991.
21. ODAM, J. Scramjet Experiments Using Radical Farming, PhD thesis, 2004,The University of Queensland, Australia.
22. ORTWERTH, P.J. *Scramjet Vehicle Integration, Scramjet Propulsion, Progress in Astronautics and Aeronautics*, AIAA Washington DC, USA, 2001, Chapter 17.
23. PANDOLFINI, P.P. Instructions for using ramjet performance analysis (RJPA) IBM-PC Version 1.0, JHU-APL NASP-86-2, 1986.
24. PAULL, A., ALESI, H. and ANDERSON, S. HyShot flight program and how it was developed, AIAA 02-4939 ,2002.
25. PINCKNEY, S.Z., FERLEMANN, S.M., MILLS, J.C. and BASS, L.S. Program manual for SRGULL version 2.0, HX#829.1, 1994.
26. PORTZ, R. and SEGAL, C. Penetration of gaseous jets in supersonic flow, *AIAA J*, 2006, **44**, (10), p 2426.
2.7 RAUSCH, V.L., MCCLINTON, C.R. and CRAWFORD, J.L. Hyper-X: flight validation of hypersonic airbreathin technology, AIAA paper 97-7024, 1997.
28. ROGERS, R.C., SHIH, A.T. and HASS, N.E. Scramjet development tests supporting the Mach 10 flight of Hyper-X, AIAA paper 2005-3351, 2005.
29. SHAPIRO, A.H. *The Dynamics and Thermodynamics of Compressible Fluid Flow*, 1953, John Wiley and Sons, New York, USA.
30. SMART, M.K. Design of three-dimensional hypersonic inlets with rectangular-to-elliptical shape transition, *J Propulsion and Power,* 1999, **15**, (3), pp 408-416.
31. SMART, M.K. Experimental testing of a hypersonic inlet with rectangular-to-elliptical shape transition, *J Propulsion and Power*, 2001, **17**, (2), pp 276-283.
32. SMART, M.K., HASS, N.E. and PAULL, A. Flight data analysis of the HyShot 2 flight experiment, *AIAA J*, 2006, **44**, (10), pp 2366-2375.
33. SMART, M.K. and RUF, E.G. Free-jet testing of a REST scramjet at off-design conditions, 2006, AIAA paper 2006-2955.
34. SMART, M.K. and TETLOW, M.R. Orbital delivery of small payloads using hypersonic airbreathing propulsion, AIAA-2006-8019, 14th AIAA/AHI Space Planes and Hypersonic Systems and Technologies Conference, 2006, Canberra, Australia.
35. STALKER, R.J., PAULL, A., MEE, D.J., MORGAN, R.G. and JACOBS, P.A. Scramjets and shock tunnels – the Queensland experience, *Progress in Aerospace Sciences*, 2006, **41**, pp 471-513.
36. STALKER, R.J. Control of hypersonic turbulent skin friction by boundary layer combustion of hydrogen, *J Spacecraft and Rockets*, 2005, **42**, (4), pp 577-587.
37. TREXLER, C.A. Inlet performance of the integrated Langley scramjet module, 1975, AIAA paper 75-3844.
38. VAN WIE, D.M. Scramjet inlets, scramjet propulsion, *Progress in Astronautics and Aeronautics*, AIAA Washington DC, USA, 2001, Chapter 7.
39. WEBBER, R.J. and MACKAY, J.S. An analysis of ramjet engines using supersonic combustion, NACA TN 4386, 1958.